Proceedings of the 3rd Croatian Conference on Earthquake Engineering - 3CroCEE
19–22 March 2025, Split, Croatia

COMBINING CONVENTIONAL AND NEXT-GENERATION INTENSITY MEASURES FOR RISK ASSESSMENT OF BRIDGES

Savvinos Aristeidou [(1)], Gerard O'Reilly [(2)]

[(1)] Postdoctoral Researcher, Scuola Universitaria Superiore IUSS Pavia, savvinos.aristeidou@iusspavia.it
[(2)] Associate Professor, Scuola Universitaria Superiore IUSS Pavia, gerard.oreilly@iusspavia.it

Abstract

This study investigates seismic risk assessment of bridge structures using a combination of conventional and next-generation intensity measures (IMs). The structures are simplified bridge models, characteristic of European construction, distinguished into regular and irregular bridges depending on the pier height arrangement. The efficacy of multiple IMs is explored, including spectral acceleration, *Sa*, significant duration, *Ds*, average spectral acceleration, Sa_{avg}, and filtered incremental velocity, *FIV*3, in predicting seismic demand. This was done by setting up different ground motion selection schemes, with different conditioning and matching IMs, and performing comparative analyses. Probabilistic seismic hazard analysis (PSHA) is conducted for each conditioning IM to obtain their seismic demand hazard curves and disaggregation. The dispersion IMs given exceedance of a range of engineering demand parameters (EDPs) was quantified, which provided a deeper understanding of the performance of each selection case across various nonlinearity levels. Our findings demonstrate that the cases conditioned on *Sa* exhibit the lowest dispersion in the elastic and early non-linear stages, making them the most reliable for low-intensity seismic events. However, as non-linearity increases, cases with Sa_{avg} as the conditioning IM demonstrate superior performance, showing the least dispersion for low to high non-linear conditions, especially in irregular bridge structures. In cases of high non-linearity and near-collapse scenarios, *FIV*3 outperforms the other IMs by offering the lowest dispersion, especially in regular bridge structures. In addition, the hazard consistency of each selection cases was checked, and a couple of examples are presented here. The case study outcomes provide valuable insights into the benefits of ground motion selection with a combination of next-generation IMs with conventional ones for seismic risk assessments. Additionally, practical guidance is offered on the leverage of recently developed generalised ground motion model (GGMM) and correlation models for achieving more accurate performance-based assessments.

Keywords: Bridges, risk assessment, generalised conditional intensity measure, intensity measures, hazard consistency

1. Introduction

Seismic risk assessment of structures, particularly bridges, has evolved significantly over the years with advancements in ground motion modelling and the development of next-generation intensity measures (IMs). Traditional approaches often relied on simpler IMs, such as *PGA*, which, while convenient, is insufficient in capturing the complex response of multi-modal and multi-component systems like bridges [1,2]. This is because other characteristics of ground motions, such as amplitude, frequency content, duration, and pulses, may significantly influence structural response. Recent research has highlighted the importance of utilising advanced IMs that better reflect the underlying seismic hazard that can be of higher engineering interest (e.g., [3,4]). These advanced (or next generation, as dubbed here) IMs not only improve the accuracy of seismic hazard representation but also enhance the reliability of risk predictions, addressing the limitations of older approaches. Building on this foundation, some IMs of engineering interest were integrated herein with advanced modelling and evaluation techniques to assess the level to which they enhance seismic risk for bridge structures.

A recently developed generalised ground motion model (GGMM) and correlation models [5,6] were leveraged to demonstrate the potential of next-generation IM. These models enabled improved predictive power and more accurate representation of seismic hazard. Also, showcased here is the practical applicability of the aforementioned models in ground motion record selection and risk assessment.

2. Ground motion selection for performance-based assessment of bridges

The selection and scaling of ground motion input are critical steps in the seismic risk analysis of bridge structures. Ground motions are typically selected and scaled based on seismic scenarios that match the site-specific hazard, coming from either probabilistic seismic hazard analysis (PSHA), or design code requirements. Scaling is usually done to achieve a specific IM value, and subsequent selection to match the spectral shape (or distribution in the probabilistic case). Many studies continue to rely on IM definitions, such as *PGA* or *Sa* at a fixed period [7–9] for regional risk assessments. Although they recognise that IMs like *PGA* are not ideal, they are often used as a baseline standard due to their simplicity and widespread adoption for convenience.

There are several ground motion selection approaches, a few of which listed and briefly described in the following. Advanced methods such as the conditional spectrum (CS) [10] and generalised conditional intensity measure (GCIM) [11] offer a rigorous probabilistic framework, with a more nuanced representation of ground motion variability by conditioning the selection process on a specific intensity measure or multiple IMs. These methods ensure consistency with the PSHA and are particularly suited for performance-based assessments. Scenario-based assessment [12], on the contrary, selects ground motions that represent specific seismic events, such as characteristic earthquakes for a known nearby fault. While this approach provides realistic inputs for scenario-specific studies, it lacks the versatility required for probabilistic risk evaluations.

3. Case study structures

3.1. Description

Seven multi-span bridges, each comprising either 4 or 8 spans of 50 m, were analysed. These bridges, previously studied by Pinho et al. [13] and O'Reilly [14], are representative of typical European bridge designs, featuring reinforced concrete (RC) piers designed according to Eurocode 8 [15]. The piers had a hollow rectangular cross-section, while the deck was continuous, with reinforcement details depicted in Figure 2(left). Pier heights were either 7 m, 14 m, or 21 m, and the bridges were categorised as regular or irregular based on the pier height variations along their length. Table 1 summarises the modal properties of the bridge structures and their classification as either regular or irregular, with additional illustrations shown in Figure 1.

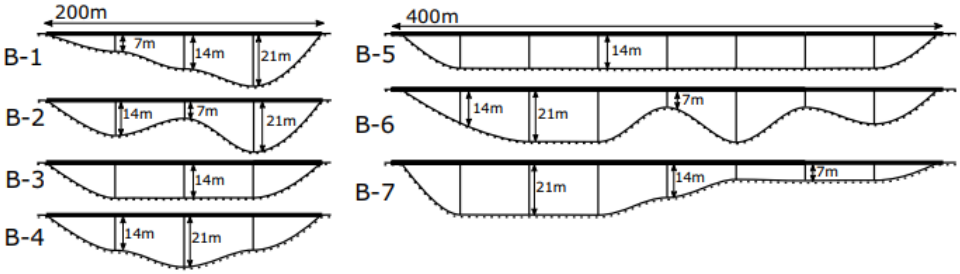

Figure 1. Illustration of the longitudinal profile of the case study bridge structures. Adapted from O'Reilly [14]

Table 1. Modal properties of each case study bridge structure

ID	Type	T_1 [s]	T_2 [s]	T_3 [s]	$\%M_1$	$\%M_2$	$\%M_3$	$\Sigma\%M$
B-1	Irregular	0.555	0.447	0.277	30	8	27	65
B-2	Irregular	0.555	0.474	0.253	30	19	5	53
B-3	Regular	0.483	0.475	0.223	32	0	66	98
B-4	Regular	0.508	0.475	0.307	6	0	77	94
B-5	Regular	0.479	0.479	0.225	16	0	76	92
B-6	Irregular	0.494	0.474	0.36	3	10	29	42
B-7	Irregular	0.556	0.436	0.387	11	7	35	53

3.2. Numerical modelling

A numerical model for each bridge was adapted to OpenSeesPy [16] from the previous OpenSees model detailed in O'Reilly [14]. The pier elements were represented using lumped plasticity models, with their parameters derived from moment–curvature analysis of the corresponding fibre-based section. This rupture strain was set at 0.10, based on Priestley et al. [17] for reinforcement steel in European bridges. The only difference from the modelling parameters described in O'Reilly and Monteiro [18] and O'Reilly [14] is the use of the *HystereticSM* material for the lumped plasticity hinges. This material was implemented with a pinching factor for deformation during reloading of 0.8, a pinching factor for force during reloading of 0.2, a damage parameter due to ductility of 0.001, and a damage parameter due to energy of 0.0001. Incorporating cyclic and in-cycle stiffness and strength degradation was essential for two main reasons: firstly, to capture the effects of matching (or not) the theoretical GCIM distribution of significant duration, *Ds*, and the implications of filtered incremental velocity, *FIV*3, matching and conditioning; and secondly, to ensure the model exhibits behaviour that more closely approximates real-world structural responses (i.e., it degrades and collapses).

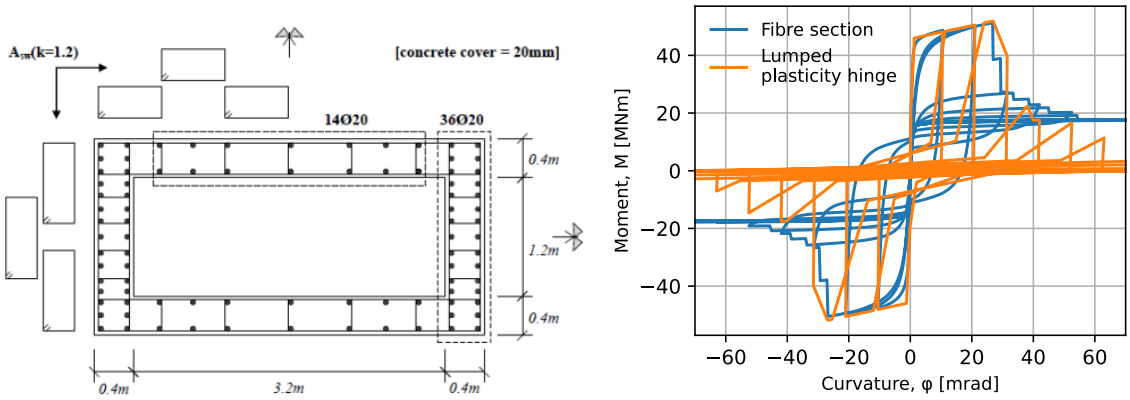

Figure 2. Illustration of structural detailing of the pier cross section [13]. The shorter side of the section is placed in the direction of the bridge deck (left). Moment curvature analysis of bottom section of the Pier with 7 m height. 10 cycles of unloading/reloading are shown here as an example, with equal curvature increments until the target curvature (right).

Modal analysis was performed to determine the dynamic properties of each bridge structure. Table 1 presents the periods, *T*, and modal masses participation factors, *M*, for the first three modes of vibration, as well as their cumulative sum for each structure, focusing exclusively on the transverse direction of response.

In bridge structures, the absence of a dominant mode or a clearly critical element complicates the selection of a suitable engineering demand parameter (EDP). Given the structural configuration of the bridges, the piers were identified as the critical elements susceptible to structural damage and element-specific EDPs were preferred. Specifically, the peak transient section curvature at the base of the piers was monitored during the ground shaking. The maximum curvature among all piers, φ_{max}, was then selected as the EDP. The curvature direction was the transversal, since in the records are applied only in the transversal direction. The collapse limit was assumed to be when the first pier reached 60 mrad of base curvature, since as seen in Figure 2(right) there is almost no moment resisting capacity in the pier at that level of deformation.

4. Hazard Analysis

PSHA was carried out for a site in Erzincan, Turkey using the OpenQuake [19] open-source software for seismic hazard and risk assessment developed by the Global Earthquake Model Foundation. The source model input was the ESHM20 model [20] and the GMM was the one developed by Aristeidou et al. [5]. Erzincan was selected as the case study site as it exhibits one of the highest seismic activities in Europe and Middle East and has been struck by a devastating 7.8 M_w earthquake in 1939, among

others. This high seismicity makes it easier to characterise the bridges' performance throughout the whole range of non-linear response without needing to reach very high return periods.

The hazard curves of each IM used to analyse bridge 1 are shown in Figure 3. The hazard curves of the IMs at other periods are omitted here for brevity but would be similar and were characterised the same way. Additionally, the hazard disaggregation of *FIV*3(0.555s) is given in Figure 4 as an example. It can be seen that most of the hazard is controlled by source-to-site distances below 30 km and magnitude mostly above 6.5. There are many scenarios contributing to the hazard, especially in low return periods, but for simplicity only the modal rupture scenario was used to select ground motions at each return period as a first-order approximation of the full disaggregation distribution.

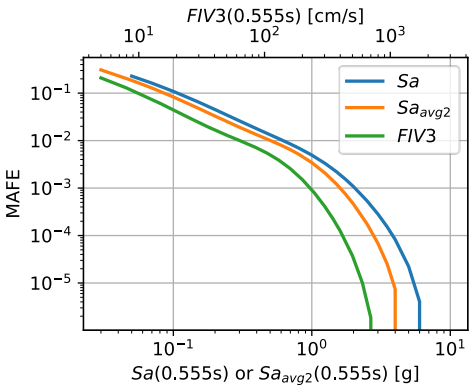

Figure 3. Hazard curves of IM* of bridge 1

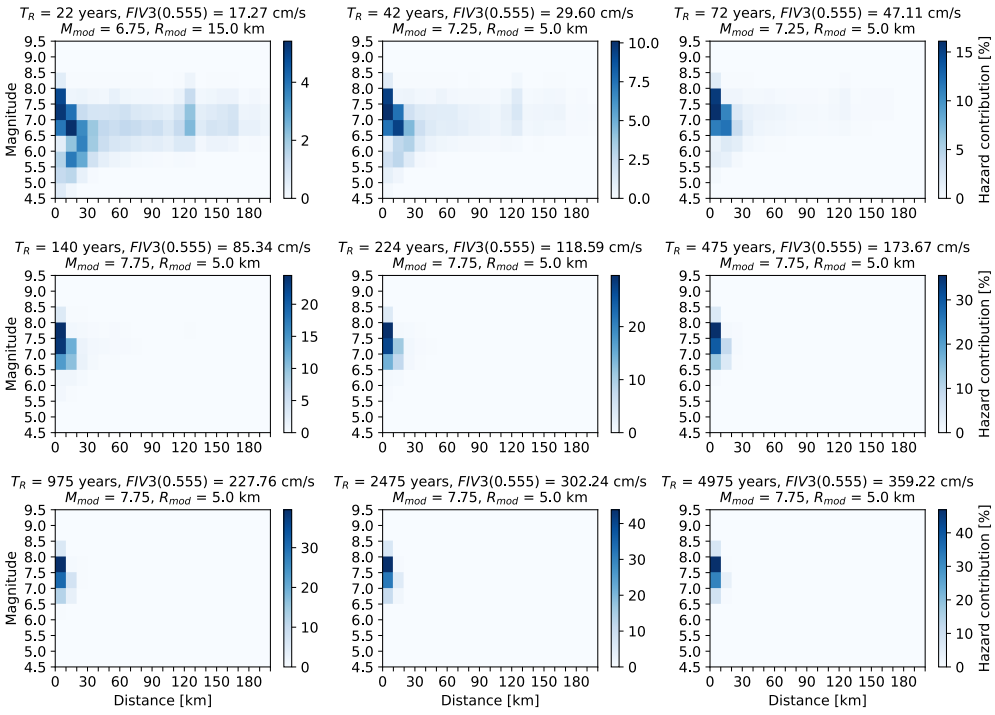

Figure 4. Hazard disaggregation of *FIV*3 at 0.555 s for the nine return periods investigated

5. Ground motion selection cases

The GCIM ground motion selection approach, introduced by Bradley [11], extends the principles of the CS approach [10] by allowing the matching IMs to differ from the conditioning IM. The CS approach is based on the assumption that spectral accelerations follow a multivariate lognormal distribution.

Building on this, the GCIM approach generalises this concept by proposing that any arbitrary vector of IMs, for a given seismic scenario, follows a multivariate lognormal distribution. Regarding the validity of this assumption, it is widely recognised that most IMs exhibit marginal lognormal distributions, as supported by regression analyses on ln(IM) in empirical GMMs. The conditional mean and standard deviation of the included IMs are therefore expressed in Equations (1) and (2).

$$\mu_{\ln IM_i|\ln IM^*,rup} = \mu_{\ln IM_i|rup} + \sigma_{\ln IM_i|rup} \cdot \rho_{\ln IM_i,\ln IM^*} \cdot \varepsilon_{\ln IM^*} \quad (1)$$

$$\sigma_{\ln IM_i|\ln IM^*,rup} = \sigma_{\ln IM_i|rup} \cdot \sqrt{1 - \rho^2_{\ln IM_i,\ln IM^*}} \quad (2)$$

where, IM_i is the matched IMs, IM* is the conditioning IM, μ is the target mean, σ is the target standard deviation, ρ the cross-correlation coefficient, and ε the normalised residual [21].

In the ground motion selection schemes investigated here, three different conditioning IMs (IM*) were included, namely $Sa(T_1)$, average spectral acceleration, $Sa_{avg2}(T_1)$, and $FIV3(T_1)$. Also, a combination of several IMs, for which the theoretical distribution was also conditionally matched (IM_i), namely $Sa(T)$, Ds_{575}, $Sa_{avg3}(T)$, $FIV3(T)$, and $Sa_{avg2}(T)$, was included. All the different ground motion record selection cases along with their conditioning and matched IMs are listed in Table 2. For the period-dependent IMs, where 'T' is denoted, it means that the whole spectrum at a range of periods was matched, and 'T_1' means that the IM at the first period of each structure was matched. It is noted here that Sa_{avg3} and Sa_{avg2} were calculated from 10 equally spanning periods ranging from $0.2T$ to $3T$, and $0.2T$ to $2T$, respectively.

Table 2. Ground motion input cases

Case No.	IM*	IMi			
0	$Sa(T_1)$	—	—	—	—
1	$Sa(T_1)$	$Sa(T)$	—	—	—
2	$Sa(T_1)$	$Sa(T)$	Ds_{575}	$Sa_{avg3}(T_1)$	$FIV3(T_1)$
3	$Sa(T_1)$	$Sa(T)$	—	$Sa_{avg3}(T_1)$	$FIV3(T_1)$
4	$Sa(T_1)$	$Sa(T)$	Ds_{575}	—	—
5	$Sa_{avg2}(T_1)$	$Sa(T)$	—	—	—
6	$FIV3(T_1)$	$Sa(T)$	—	—	—
7	$Sa_{avg2}(T_1)$	—	—	$Sa_{avg2}(T)$	—
8	$FIV3(T_1)$	—	—	—	$FIV3(T)$
9	$Sa_{avg2}(T_1)$	—	Ds_{575}	$Sa_{avg2}(T)$	—
10	$FIV3(T_1)$	—	Ds_{575}	—	$FIV3(T)$

No rupture parameter limits were applied in the selection of ground motions, but a maximum scale factor of 8 was set. Both horizontal components of the pool of recorded motions were included in the selection pool, in other words the number of possible ground motions to be used for the analysis was double the number of available recordings. This is done because the bridge is excited unidirectionally (transversally). A set of 50 records were selected for each stripe.

The hazard consistency was checked for the ground motion selection cases and two examples are illustrated in Figure 5. The checks are shown for four different periods of Sa, a shorter period than the conditioning one, a period that is close to the conditioning, and two longer periods than the conditioning one. Firstly, it can be observed that the selection Case 0 gives a good match with the seismic hazard curves, except for $T = 0.2$ s, which is an unexpected result since no effort was made in the selection to achieve hazard consistency. It seems to be a circumstantial result, emanating from the interaction between the lower medians and higher dispersions of the selected records of Case 0. This is the case for longer periods than the conditioning one (spectrum not shown here due to space limitations). For shorter periods than the conditioning, it can be seen that the selected records present higher hazard curve than that from PSHA. This is because, while the median of selected records is close in value to the target median, the dispersion of the selected records is higher that the target dispersion.

Figure 5(right) illustrates the hazard consistency check of ground motion record selection Case 5, which is conditioned on Sa_{avg2}. It can be seen that there is a good match with the hazard curves obtained from PSHA, except for the high annual rate of exceedance part of $T = 2$ s. The source of this mismatch is due to the fact that not all input parameters of the GGMM could be extracted from the hazard disaggregation, only magnitude and distance, therefore some assumptions had to be made for other parameters. Another reason is the choice of the modal scenario of the hazard disaggregation, and not the inclusion of all the scenarios that significantly contribute to hazard.

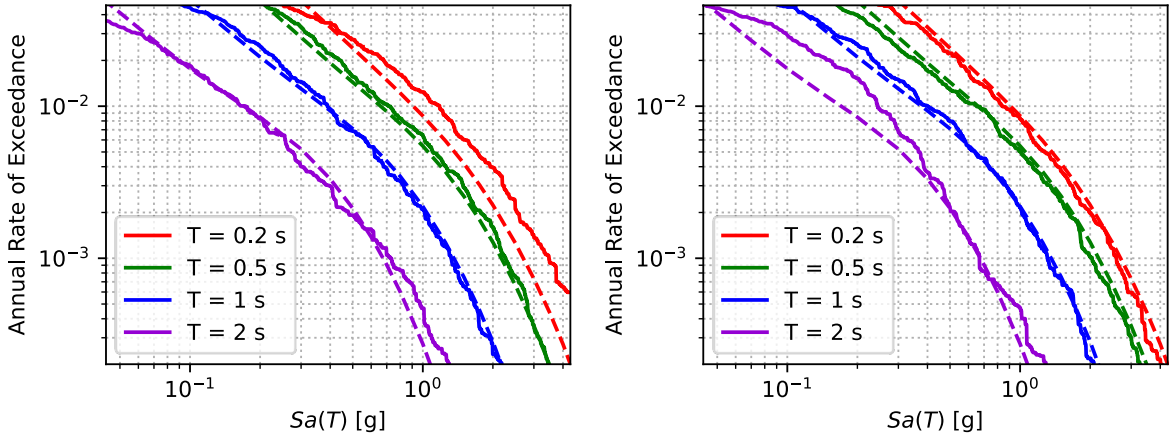

Figure 5. Hazard consistency checks for ground motion input Cases 0 (left) and 5 (right) for bridge B-1. Dashed lines represent the hazard curves and solid lines represent the reconstructed hazard curves obtained from the selected ground motions

6. Results

6.1. Multiple stripe analysis (MSA) results

With the ground motion record sets identified for each selection case, return period, and bridge structure, MSA was carried on the numerical model of each bridge structure. The output of this analysis is an empirical distribution of the bridge response, characterised via an EDP (in this case φ_{max}), versus an IM level corresponding to a specific return period. As an example, the MSA results for the case study bridge B-1 and ground motion selection Case 5 are illustrated in Figure 6. The response ordinates of only the non-collapse cases are shown in the plot, for which the logarithmic mean and ±1 standard deviation are also illustrated. Also shown in the right-hand side of the figure is the probability of collapse in each intensity level.

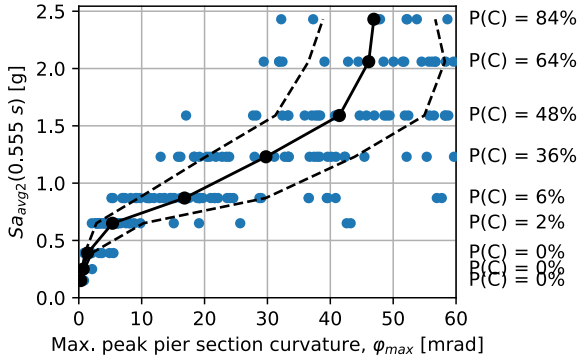

Figure 6. MSA results obtained with the ground motion input 5 on case study bridge B-1. Also depicted is the logarithmic mean and ±1 standard deviation of the non-collapse cases, and the probability of collapse resulting from each intensity level

6.2. Demand-based evaluation

The probability of an IM causing exceedance of certain damage limit threshold, which is indexed by an EDP value, is often modelled using a lognormal distribution characterised by a median, $\eta_{IM|EDP}$, and dispersion, $\beta_{IM|EDP}$, forming what is known as a seismic fragility function. By integrating this function with the mean hazard curve derived from PSHA, $H(im)$, the mean annual frequency of exceedance (MAFE) of that EDP value is obtained, offering a more comprehensive and consistent measure of seismic risk. The calculation of this MAFE is given in Equation (3), where $\Phi[\cdot]$ represents the standard normal cumulative distribution function.

$$\lambda = \int_0^\infty \Phi\left[\frac{\ln im - \eta_{IM|EDP}}{\beta_{IM|EDP}}\right] |dH(im)| \tag{3}$$

The parameter $\beta_{IM|EDP}$ in Equation (3) is plotted in Figure 7 versus the whole range of EDP response of the structure. The legend indicates each case, with its corresponding short naming scheme. The first IM is the conditioning one, while the IMs after the dash symbol are the ones whose theoretical GCIM distribution is been matched by the record selection. The IMs after the dash that are denoted with "(T)" are the ones whose spectrum is matched, whereas for the other period-dependent IMs, without "(T)", only at the 1st period of each structure was matched For the regular bridge structures (B-3, B-4, and B-5), Cases 6, 8, and 10 exhibit the lowest dispersion $\beta_{IM|EDP}$ for φ_{max} values exceeding 10 mrad, which spans most of the response range. These cases employ *FIV*3 as the IM*. Among these, Case 10 clearly achieves the lowest dispersion overall by conditioning on *FIV*3 and matching both the *FIV*3 spectrum and Ds_{575}, demonstrating its superior efficiency for these regular bridges, especially for the higher levels of EDP when the structure is responding in its non-linear range since the yield curvature was approximately 1.25 mrad.

In contrast, for the irregular bridge structures, Cases 5, 7, and 9 show the lowest dispersion, particularly in the initial half of the structural response range. These cases condition on $Sa_{avg2}(T_1)$. While the differences among these cases are not pronounced, Case 9 stands out as slightly more efficient. This can be attributed to its matching of the expected duration distribution at the site, which additionally ensures more accurate median response estimates.

For cases using *Sa* as the conditioning IM, dispersion remains low in the initial stages of the response but increases significantly as the structural response becomes more non-linear. Cases 1 and 3 exhibit the highest dispersion, although they differ little from Cases 2 and 4. Interestingly, Case 0—the most basic scenario—exhibits lower dispersion than the other *Sa*-conditioned cases, despite its higher dispersion of the selected records. This unexpected outcome can be explained by the inclusion of records with lower spectral ordinates in longer periods and also lower durations, which artificially raises the efficiency of *Sa* as a conditioning IM. However, this comes at the expense of not adhering to hazard consistent selection rules, as Case 0 fails to represent the site-specific hazard and underestimates risk, particularly at higher EDPs where structural nonlinearity and longer-period motions dominate, as discussed in Section 5.

Finally, it is worth noting that cases incorporating *Ds* as a matched IM consistently achieve lower dispersion compared to corresponding cases where *Ds* is not matched. This highlights the value of including duration-based IMs, like *Ds*, in reducing variability and improving the accuracy of seismic demand predictions.

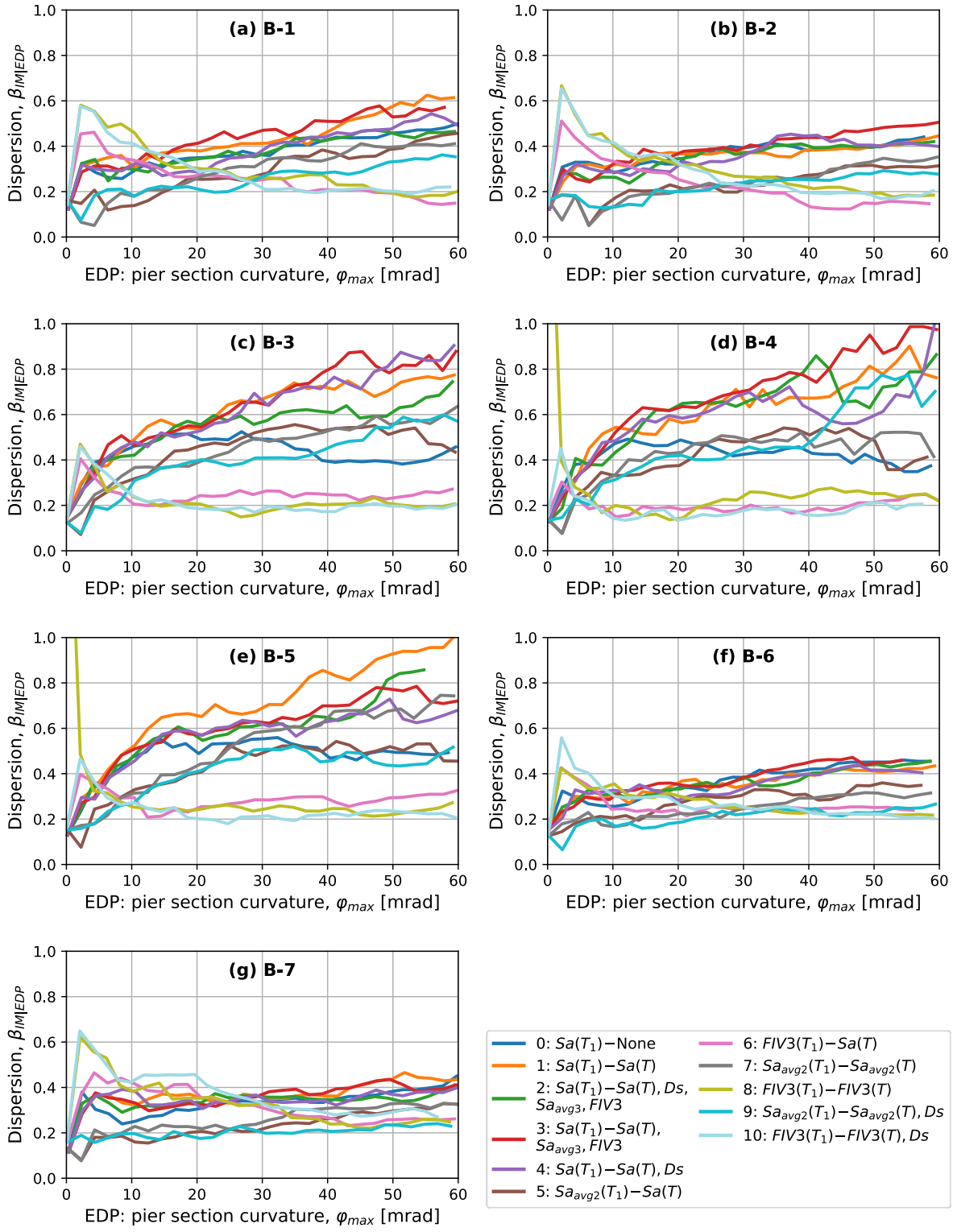

Figure 7. Dispersion of IM given exceedance of EDP

6.3. Risk-based evaluation

It is expected that for the hazard-consistent selection cases the resulting MAFE estimates converge to a similar value for each bridge. These curves can be compared and, in some cases, validated against

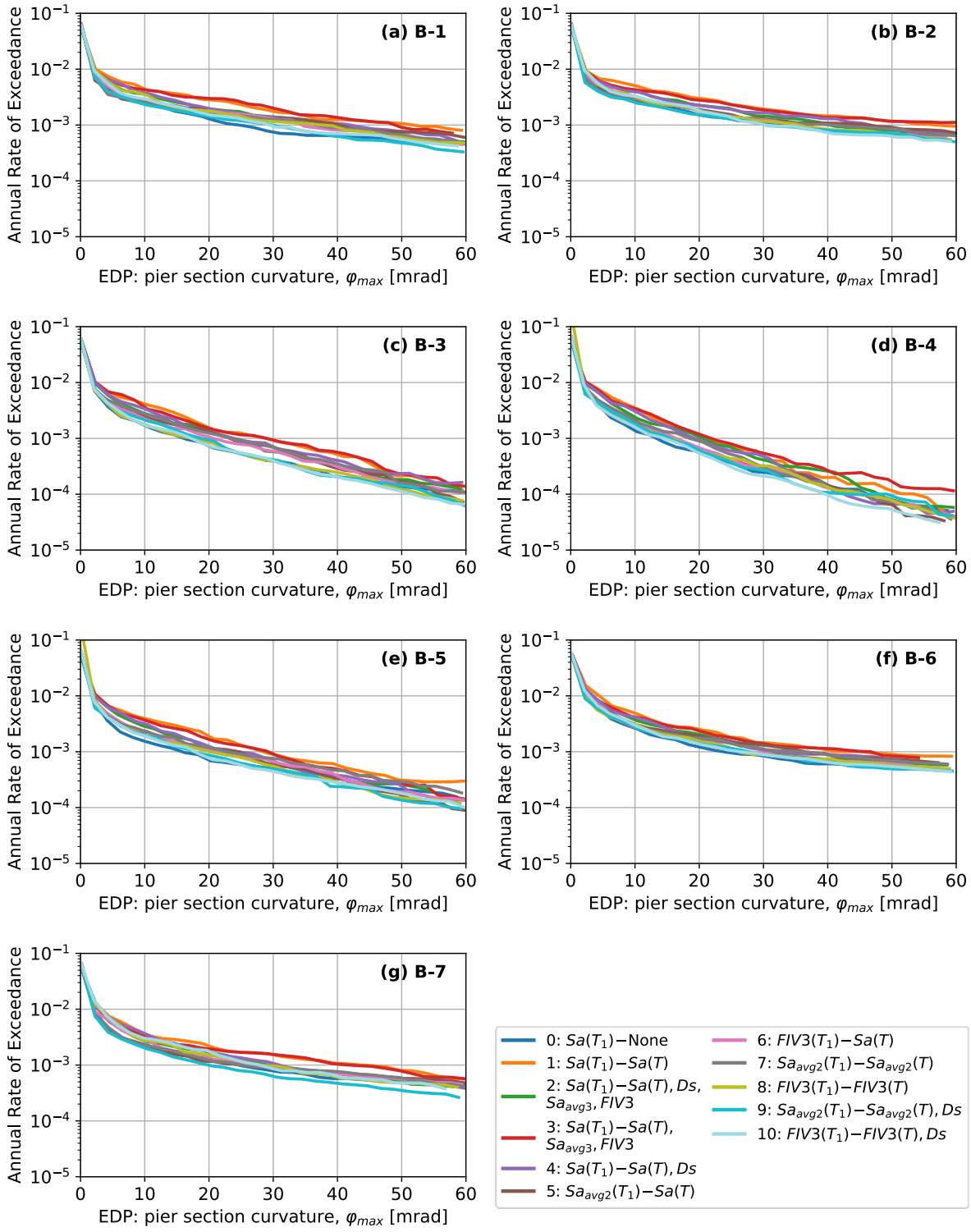

Figure 8. Seismic demand hazard curves of the case study bridges

results from detailed physics-based simulations, as discussed by Bradley et al. [22]. However, such validations would be beyond the scope of this study.

From Figure 8, there are a number of observations that can be made. Regular bridges have lower MAFE, than the irregular bridges, especially in higher EDPs. B-4 has the lowest risk. Cases 1 and 3 consistently gave higher estimates of λ in all the bridge structures. It is interesting to note the Cases 2 and 4 (i.e.,

conditioning on *Sa* and matching the Ds_{575}) result in MAFE closer to the rest of the cases, which indicates that matching the Ds_{575} GCIM distribution alleviates part of the incompetencies of *Sa* as a conditioning IM. Case 0 gives one of the lowest risk estimates because of its lower-than-expected *Sa* spectrum and Ds_{575} of the records, as already discussed above, hence deeming it the ``worst'' case for what concerns risk estimation.

The difference between Cases 5 and 7 is negligible. The same applies to Cases 6 and 8, which indicates that there is no practical difference in matching the *Sa* or Sa_{avg2} spectrum along with conditioning on Sa_{avg2}, or matching the *Sa* or *FIV*3 spectrum along with conditioning on *FIV*3. This is likely due to the high level of correlation between each of these IMs [6], meaning that these cases are slight variations of each other. It also underlines the importance of hazard-consistent ground motion record selection when compared to Case 0, for example.

Additionally, Cases 9 and 10 give similar MAFE estimates, which are relatively low in value compared to the rest of the cases. All in all, it can be concluded that matching the Ds_{575} distribution makes a notable difference in the risk estimates and is likely what should be focused on for analysts when dealing with non-linear systems with some form of strength degradation.

7. Summary and conclusions

In this conference paper, an analysis was conducted to evaluate the implications of next-generation IMs on the seismic risk assessment of bridge structures. The GGMM and correlation models, developed by Aristeidou et al. [5,6], were employed to facilitate the seismic hazard analyses and selection of ground motions using advanced approaches, such as the GCIM method. The latter approach ensures that key features of ground motions beyond spectral acceleration, such as duration and velocity, are appropriately represented and matched during selection. Ground motion records were selected and scaled according to different strategies, including just scaling to the conditioning IM, CS-based and GCIM-based selection. A suite of multi-span bridge structures with varying pier heights and span configurations was analysed using numerical models built in OpenSeesPy. The MSA method was used to quantify structural demands, and risk estimates were derived for the case study bridges.

Several ground motion selection cases were investigated and the following conclusions regarding the comparisons between them are outlined:

- Cases 0 and 1: Case 0 gave lower IM dispersion for a given EDP exceedance for the majority of EDP range. Additionally, its lower-than-expected *Sa* spectrum was primarily responsible for the lower risk estimates. This highlights the importance of matching target distributions of all pertinent IMs, and not just the conditioning one.
- Cases 1 and 2: The CS approach gave ground motions with higher-than-expected Ds_{575}, which resulted in higher EDP medians, and therefore risk estimates. The dispersions were somewhat lower in Case 2, and therefore presented higher efficiency. Nevertheless, the differences in dispersion were small.
- Cases 1, 2, 3, and 4: Cases 2 and 4 give similar results, while Cases 1 and 3 also exhibit similar results between them. Therefore, we can conclude that the differences between Cases 1 and 2 come solely from matching or not the Ds_{575}.
- Cases 1, 5, and 6: Case 1 resulted in low dispersion only in the initial stages of EDP response, which is the elastic and mildly inelastic stage, and then the dispersion quickly rises. Case 5 was more efficient in the irregular bridges, while Case 6 dominated with regards to efficiency in most of the non-linear response range of the regular bridges.
- Cases 5 and 7: Dispersions and risk estimates are very similar between the two cases. Which suggests that one can select any of the two selection schemes and obtain very similar results.
- Cases 6 and 8: Dispersions and risk estimates are very similar between the two cases, with Case 6 resulting in slightly lower dispersions. This suggests that when conditioning on *FIV*3, matching the *Sa* spectrum will give slightly more accurate results, than matching the *FIV*3 spectrum.

- Cases 9 and 10, versus all the rest: The CS of Sa_{avg2} and *FIV*3 while matching the Ds_{575} theoretical distribution at the site seem to be best cases. Case 9 was found to be more accurate for the initial and intermediate stages of nonlinearity, while Case 10 was found to be more accurate for the deeper stages of response nonlinearity and near collapse.

By utilising a newly developed GGMM and correlation models, the practical benefits of next-generation IMs, such as *FIV*3 and Sa_{avg2}, in improving both the accuracy and consistency of seismic demand predictions were demonstrated. Specifically, the GCIM-based approach proved highly effective in reducing the dispersion of structural response while maintaining hazard consistency—a critical factor often overlooked in traditional selection methods. The findings further highlighted the sensitivity of IM's performance to structural regularity, with velocity-based IMs like *FIV*3 excelling for regular bridges and Sa_{avg2} exhibiting superior performance for irregular structures.

Overall, this work bridges the gap between state-of-the-art ground motion selection techniques and practical applications for researchers and practitioners who would like to use the IMs utilised here. The tools and methodologies used here can serve as a foundation for future research and implementation in performance-based designs and assessments.

Acknowledgements

This work has been developed within the framework of the projects "Dipartimenti di Eccellenza", funded by the Italian Ministry of Education, University and Research at IUSS Pavia. The authors would also like to acknowledge Davit Shahnazaryan for developing the ground motion selection tool used in this study.

References

1. Luco N, Cornell CA. Structure-specific scalar intensity measures for near-source and ordinary earthquake ground motions. *Earthquake Spectra* 2007; **23**(2): 357–392. DOI: 10.1193/1.2723158.
2. Huang Q, Gardoni P, Hurlebaus S. Probabilistic Seismic Demand Models and Fragility Estimates for Reinforced Concrete Highway Bridges with One Single-Column Bent. *Journal of Engineering Mechanics* 2010; **136**(11): 1340–1353. DOI: 10.1061/(ASCE)EM.1943-7889.0000186.
3. Kohrangi M, Vamvatsikos D, Bazzurro P. Pulse-like versus non-pulse-like ground motion records: Spectral shape comparisons and record selection strategies. *Earthquake Engineering and Structural Dynamics* 2019; **48**(1): 46–64. DOI: 10.1002/eqe.3122.
4. Dávalos H, Miranda E. Evaluation of FIV3 as an Intensity Measure for Collapse Estimation of Moment-Resisting Frame Buildings. *Journal of Structural Engineering* 2020; **146**(10): 1–14. DOI: 10.1061/(asce)st.1943-541x.0002781.
5. Aristeidou S, Shahnazaryan D, O'Reilly GJ. Artificial neural network-based ground motion model for next-generation seismic intensity measures. *Soil Dynamics and Earthquake Engineering* 2024; **184**: 108851. DOI: 10.1016/j.soildyn.2024.108851.
6. Aristeidou S, Shahnazaryan D, O'Reilly GJ. Correlation Models for Next-Generation Amplitude and Cumulative Intensity Measures using Artificial Neural Networks. *Earthquake Spectra* 2024; **0**(0): 1–24. DOI: 10.1177/87552930241270563.
7. HAZUS. *Multi-hazard loss estimation methodology - earthquake model,*. Washington, DC, USA: 2003.
8. Villar-Vega M, Silva V, Crowley H, Yepes C, Tarque N, Acevedo AB, *et al.* Development of a Fragility Model for the Residential Building Stock in South America. *Earthquake Spectra* 2017; **33**(2): 581–604. DOI: 10.1193/010716EQS005M.
9. Del Gaudio C, De Martino G, Di Ludovico M, Manfredi G, Prota A, Ricci P, *et al.* Empirical fragility curves from damage data on RC buildings after the 2009 L'Aquila earthquake. *Bulletin of Earthquake Engineering* 2017; **15**(4): 1425–1450. DOI: 10.1007/s10518-016-0026-1.
10. Baker JW. Conditional Mean Spectrum: Tool for Ground-Motion Selection. *Journal of Structural Engineering* 2011; **137**(3): 322–331. DOI: 10.1061/(asce)st.1943-541x.0000215.

11. Bradley BA. A generalized conditional intensity measure approach and holistic ground-motion selection. *Earthquake Engineering and Structural Dynamics* 2010; **39**(12): 1321–1342. DOI: 10.1002/eqe.995.

12. Tarbali K, Bradley BA. Ground motion selection for scenario ruptures using the generalised conditional intensity measure (GCIM) method. *Earthquake Engineering & Structural Dynamics* 2015; **44**(10): 1601–1621. DOI: 10.1002/eqe.2546.

13. Pinho R, Monteiro R, Casarotti C, Delgado R. Assessment of continuous span bridges through nonlinear static procedures. *Earthquake Spectra* 2009; **25**(1): 143–159. DOI: 10.1193/1.3050449.

14. O'Reilly GJ. Seismic intensity measures for risk assessment of bridges. *Bulletin of Earthquake Engineering* 2021; **19**(9): 3671–3699. DOI: 10.1007/s10518-021-01114-z.

15. CEN. *Eurocode 8: Design of Structures for Earthquake Resistance - Part 2: Bridges (EN 1998–2:2005)*. Brussels, Belgium: 2005.

16. Zhu M, McKenna F, Scott MH. OpenSeesPy: Python library for the OpenSees finite element framework. *SoftwareX* 2018; **7**: 6–11. DOI: 10.1016/j.softx.2017.10.009.

17. Priestley MJN, Seible F, Calvi GM. *Seismic design and retrofit of bridges*. New York: John Wiley & Sons; 1996. DOI: 10.1002/9780470172858.

18. O'Reilly GJ, Monteiro R. On the efficient risk assessment of bridge structures. *COMPDYN Proceedings*, vol. 1, 2019. DOI: 10.7712/120119.6933.18933.

19. GEM. The OpenQuake-engine User Manual. *Global Earthquake Model (GEM) OpenQuake Manual for Engine Version 3180* 2022. DOI: 10.13117/GEM.OPENQUAKE.MAN.ENGINE.3.18.0.

20. Danciu L, Nandan S, Reyes C, Basili R, Weatherill G, Beauval C, *et al.* The 2020 update of the European Seismic Hazard Model: Model Overview 2021(EFEHR Technical Report 001 v1.0.0): 1–121.

21. Baker JW, Cornell CA. Spectral shape, epsilon and record selection. *Earthquake Engineering & Structural Dynamics* 2006; **35**(9): 1077–1095. DOI: 10.1002/eqe.571.

22. Bradley BA, Burks LS, Baker JW. Ground motion selection for simulation-based seismic hazard and structural reliability assessment. *Earthquake Engineering & Structural Dynamics* 2015; **44**(13): 2321–2340. DOI: 10.1002/eqe.2588.